Available online at www.sciencedirect.com

ScienceDirect

Ceramics International 39 (2013) 9293–9298

CERAMICS INTERNATIONAL

www.elsevier.com/locate/ceramint

Core–shell $BaMoO_4$@SiO_2 nanospheres: Preparation, characterization, and optical properties

Jiasheng Wang, Xin Li, Limei Luo, Shufen Zhang, Rongwen Lu*

State Key Laboratory of Fine Chemicals, Dalian University of Technology, Dalian 116024, PR China

Received 30 March 2013; received in revised form 2 May 2013; accepted 13 May 2013
Available online 21 May 2013

Abstract

Core–shell $BaMoO_4$@SiO_2 nanospheres were prepared in reverse microemulsions and exhibited enhanced photoluminescence (PL) intensity as compared to that of the uncoated $BaMoO_4$. Characterization was performed using transmission electron microscopy (TEM), high-resolution transmission electron microscopy (HRTEM), selected area electron diffraction (SAED), energy-dispersive X-ray spectroscopy (EDX), and X-ray powder diffraction (XRD). It was found that the silica shell could increase the PL intensity, but the shell is not the thicker the better. The PL emission can be decomposed into three individual Gaussian components: two UV emissions at 308 nm and 369 nm and a visible emission at 448 nm. Such short emission wavelengths can be attributed to quantum size effect of the small $BaMoO_4$ cores (~16 nm).

Keywords: A. Powders: chemical preparation; B. Nanocomposites; C. Optical properties; D. SiO_2

1. Introduction

As an important type of inorganic luminescent materials, molybdates and tungstates with large bivalent cations (ABO_4, ionic radius > 0.099 nm, A = Ca, Sr, Ba, Pb; B = Mo, W), existing in the scheelite structure, have a high potential for applications in many fields, such as light-emitting diodes, solid-state lasers, and scintillation detectors [1–6]. Among these compounds, barium molybdate ($BaMoO_4$) has been widely investigated because of its attractive photoluminescence (PL) [7–10]. However, practical applications of pure $BaMoO_4$ have rarely been reported due to the unsatisfying PL intensity. Thus, it is still highly needed to develop a facile method to enhance it. On the other hand, UV light-emitting materials have attracted considerable interest recently due to the demand for optoelectronic devices, such as UV light-emitting diodes, laser diodes, faster laser typing, and higher-density information storage [11–14]. Thus, it would be very meaningful to prepare materials with PL emissions mainly in the UV region. As the $BaMoO_4$ particles decrease in size from 1300 nm [15] to 30 nm [7], their maximum PL emission peaks have a blue shift from 542 nm to 400 nm, showing obvious quantum size effect. Therefore, preparing $BaMoO_4$ with sizes < 30 nm would be a feasible way to obtain UV emission.

Since the 1990 s [16], core–shell structures have been popular in the nano field because of their superior physical and chemical properties compared to their single-component counterparts [17]. Among these core–shell structures, silica-coated nanoparticles have become increasingly important in various fields since their introduction by Liz-Marzán et al. [18] in 1996. Due to its optical transparency, chemical inertness, and controlled porosity, silica has been frequently used as a shell to improve the properties of the core materials, such as the photostability of quantum dots [19], the stability of catalysts [20], and the biocompatibility of nanoprobes [21]. It is of special interest that silica coating can enhance the PL intensity of luminescent materials, as observed by Kuang [22], Zhou [23], and Lu [24,25]. Keeping this in mind, we intend to synthesize core–shell $BaMoO_4$@SiO_2 and investigate the effect of coating on its PL property.

In the last decade, various methodologies for the silica coating of nanoparticles have been developed [21,26]. Of these methods, reverse microemulsions, as thermodynamically stable, transparent, and isotropic liquid media with nanosized water pools, are particularly powerful [27–29]. In addition to their advantages of being easy to handle, demanding no extreme pressure or temperature, and requiring no special or expensive equipment, their shape and size can also be readily controlled by adjusting

*Corresponding author. Tel.: +86 411 84986270; fax: +86 411 84986292.
E-mail address: lurw@dlut.edu.cn (R. Lu).

0272-8842/$ - see front matter © 2013 Elsevier Ltd and Techna Group S.r.l. All rights reserved.
http://dx.doi.org/10.1016/j.ceramint.2013.05.043

their compositions [30]. We thus adopted a reverse microemulsion strategy to synthesize the core–shell $BaMoO_4@SiO_2$.

In this work, we prepared core–shell $BaMoO_4@SiO_2$ nanocomposites in a reverse microemulsion of Brij-58/cyclohexane/water and investigated their optical properties. The PL intensity was enhanced by silica coating and the main PL emission peaks entered UV region.

2. Experimental

2.1. Materials

Polyoxyethylene (20) cetyl ether (Brij-58) was purchased from Acros. Tetraethyl orthosilicate (TEOS), ammonium hydroxide ($NH_3 \cdot H_2O$, 25–28%), sodium molybdate ($Na_2MoO_4 \cdot 2H_2O$), barium chloride ($BaCl_2 \cdot 2H_2O$), cyclohexane, and isopropanol (IPA) were purchased from Sinopharm Chemical Reagent Co. Ltd. (SCRC). All chemicals were of analytical grade and used without further purification. Deionized water (18.2 MΩ) was used as necessary.

2.2. Synthesis of $BaMoO_4@SiO_2$

In a typical synthesis, 3.37 g of Brij-58 (3 mmol) was added to 15 mL of cyclohexane in a 50-mL two-necked round-bottom flask, heated to 50 °C with stirring until the mixture became transparent. Then 0.45 mL of a sodium molybdate solution (1 M) was added to form a reverse microemulsion. After 1 h of stirring, 0.45 mL of barium chloride solution (1 M) was added dropwise. After another hour, 1.2 mL of ammonium hydroxide was added dropwise. Half an hour later, either 1 g or 2 g of TEOS (in different experiments) was added into the system. The silica-coating process was allowed to proceed for 2 h, after which 15 mL of IPA was added for demulsification. After ultrasonication for 5 min, the mixture was centrifuged at 6000 rpm for 10 min. The precipitate was washed twice with IPA, dried at 100 °C in an oven for 10 h, and then calcined at 500 °C for 2 h under an air stream. Uncoated $BaMoO_4$ were obtained by repeating the same procedure without the addition of ammonium hydroxide and TEOS.

2.3. Characterization

TEM was performed at room temperature on a JEOL transmission electron microscope (JEM-2000 EX) using an accelerating voltage of 120 kV. High-resolution transmission electron microscopy (HRTEM), selected area electron diffraction (SAED), and energy-dispersive X-ray spectroscopy (EDX) were conducted on an FEI Tecnai G2 F20 microscope working at 200 kV. The XRD patterns were recorded on a SHIMADZU X-ray diffractometer (XD-3A) with Cu-Kα

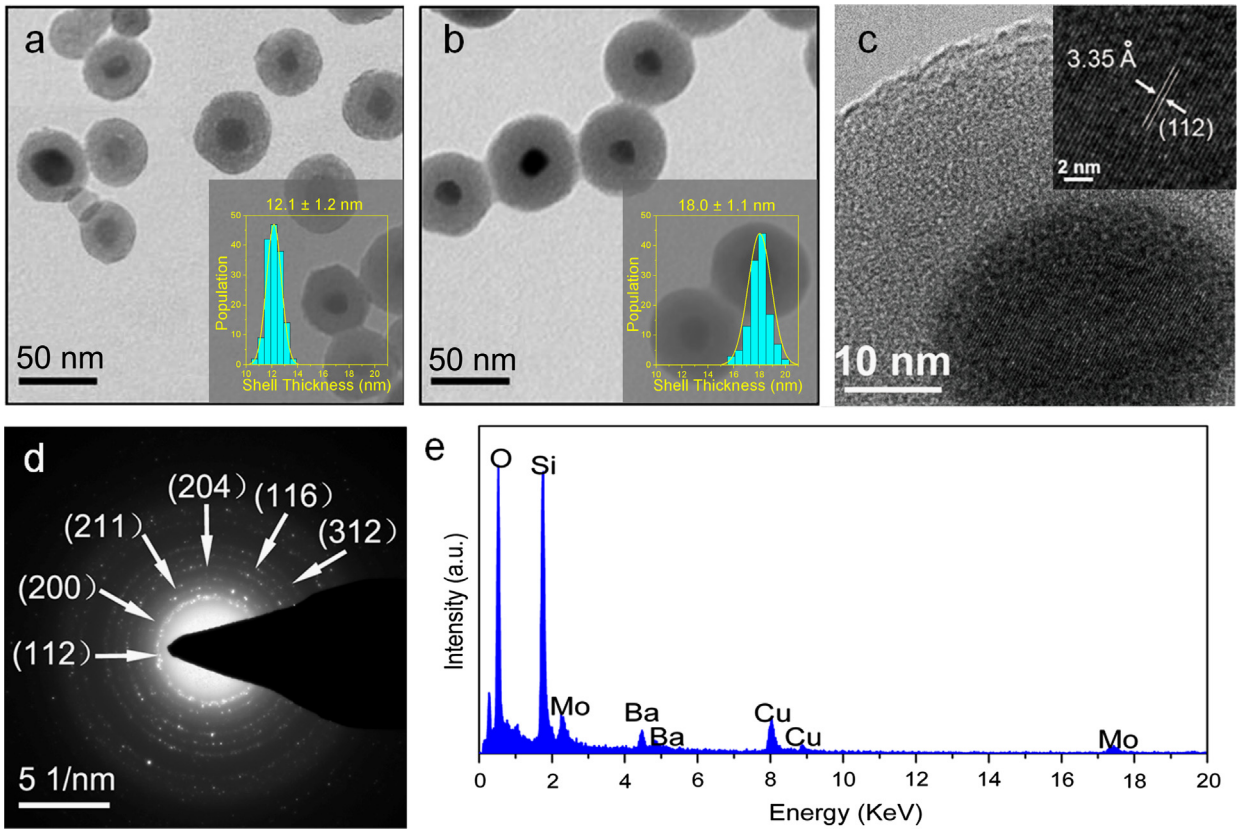

Fig. 1. TEM images of $BaMoO_4@SiO_2$ with TEOS amounts of (a) 1.0 g and (b) 2.0 g. The insets in (a) and (b) are corresponding shell thickness distribution histograms. (c) HRTEM image, (d) SAED pattern and (e) EDX spectrum of BaMoO4@SiO2 with 2.0 g of TEOS. The inset in (c) shows the fringes of the core at higher magnification.

(0.1542 nm) radiation, scanning from 10° to 70° (2θ) at a rate of 6°/min.

2.4. Optical properties test

40 mg of uncoated $BaMoO_4$ was dispersed in 900 mL of water, transferred into a 1000-mL volumetric flask, diluted with water to volume and tested on UV–vis spectrophotometer (Agilent 8453). According to the UV–vis spectrum, the maximum absorption wavelength of $BaMoO_4$ was 209 nm, and the absorbance value was 0.96. To compare the PL intensity, the concentrations of the core–shell $BaMoO_4@SiO_2$ materials were adjusted to fix the absorbance at 209 nm to the same value, i.e., 0.96. A PL spectrometer (Hitachi F-7000) was used to test PL intensity at room temperature.

3. Results and discussion

3.1. Characterization of nano core–shell $BaMoO_4@SiO_2$

Fig. 1a and b show typical TEM images and corresponding shell thickness distribution histograms of core–shell $BaMoO_4@SiO_2$ with different TEOS amounts. The size of the $BaMoO_4$ cores in both core–shell structures is 16–17 nm, endowing them with the potential for UV emission because of the quantum size effect (the wavelength of the PL emission for 30 nm $BaMoO_4$ is 400 nm [7]). Silica shell thickness increases with the increased amounts of TEOS. The core–shell nanostructures possess shell thicknesses of 12.1 ± 1.2 nm and 18.0 ± 1.1 nm for 1 g and 2 g of TEOS, respectively. For convenience, hereinafter the thicknesses are referred to as 12 nm and 18 nm, respectively.

The HRTEM image, SAED pattern, and EDX spectrum of $BaMoO_4@SiO_2$ are shown in Fig. 1c–e. From the HRTEM we can see clear fringes of the lattice planes (marked by white short parallel lines in the inset) on the core, indicating high crystallinity of the $BaMoO_4$ cores. The interplanar distance of 3.35 Å can be attributed to scheelite $BaMoO_4$ (112). The SAED pattern exhibits a number of bright spots arranged in concentric rings, which correspond to the (112), (200), (211), (204), (116), and (312) planes of scheelite $BaMoO_4$. Among those planes, (112) is the brightest one, indicating its predominance. In the EDX spectrum, peaks of Ba, Mo, O, and Si are observed, while the Cu signal is ascribed to the copper grid for supporting the sample. These results amply demonstrate the high crystallinity and composition correctness of our product.

The phase structures of the as-synthesized samples were characterized using powder X-ray diffraction (XRD). Fig. 2 shows diffraction patterns of $BaMoO_4@SiO_2$ with different shell thicknesses. All the peaks can be indexed to the pure scheelite structure of $BaMoO_4$ (JCPDS Card no. 29-0193). The dominant plane is (112), which agrees well with the HRTEM result and electron diffraction data (Fig. 1c and d). The size of $BaMoO_4$ cores was calculated to be 16.6 nm by the Debye–Scherrer formula, also in good agreement with those observed in TEM images (Fig. 1a and b). Pure amorphous silica was analyzed by XRD for comparison and showed a broad hump between 20° and 30°, as shown in Fig. 2. Such a hump could be identified in the XRD patterns of $BaMoO_4@SiO_2$ with different shell thicknesses. The intensity of the hump is very weak compared to that of $BaMoO_4$ due to the amorphous state of silica. However, a slight increase of the hump still can be identified with the increase of the shell thickness, implying the increase of SiO_2 mass fraction in the composites.

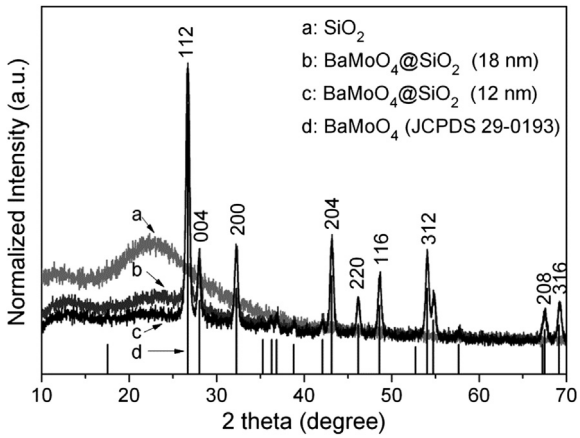

Fig. 2. XRD patterns of (a) pure silica, (b) $BaMoO_4@SiO_2$ with shell thickness of 18 nm, (c) $BaMoO_4@SiO_2$ with shell thickness of 12 nm, and (d) Literature data for pure $BaMoO_4$ (JCPDS No. 29-0193).

3.2. Formation mechanism of the core–shell structures

In order to investigate the formation mechanism of the core–shell structures, we analyzed the intermediates (i.e., the uncoated $BaMoO_4$ and coated but not calcined $BaMoO_4$) by XRD and HRTEM. The results, together with those of the final products (take the $BaMoO_4@SiO_2$ with 18 nm shell as an example), are shown in Fig. 3. From the XRD patterns, we can see that before silica coating, $BaMoO_4$ has been formed (Fig. 3a). The weak intensity and broadening of the diffraction peaks suggested low crystallinity. After silica coating, the diffraction peaks (Fig. 3b) showed little difference except the appearance of a broad hump between 20° and 30°, which can be attributed to silica. After calcination, the diffraction peaks became narrow and the intensity was significantly increased (Fig. 3c), indicating high crystallinity was obtained. The same results can be concluded from HRTEM images (Fig. 3d–f), where we can see that after calcination the fringes of the lattice planes appeared (Fig. 3f), which could not be observed before calcination, further proving that calcination can increase the crystallinity of the cores.

Based on the above analysis, the formation mechanism of the core–shell $BaMoO_4@SiO_2$ nanocomposites is proposed and illustrated in Scheme 1. Firstly the microemulsion was formed by Brij-58, cyclohexane, and Na_2MoO_4 solution. The MoO_4^{2-} was confined in the water pools. Once $BaCl_2$ solution was added, $BaMoO_4$ cores were precipitated out, which can be confirmed by the XRD pattern of Fig. 3a. Then silica shell

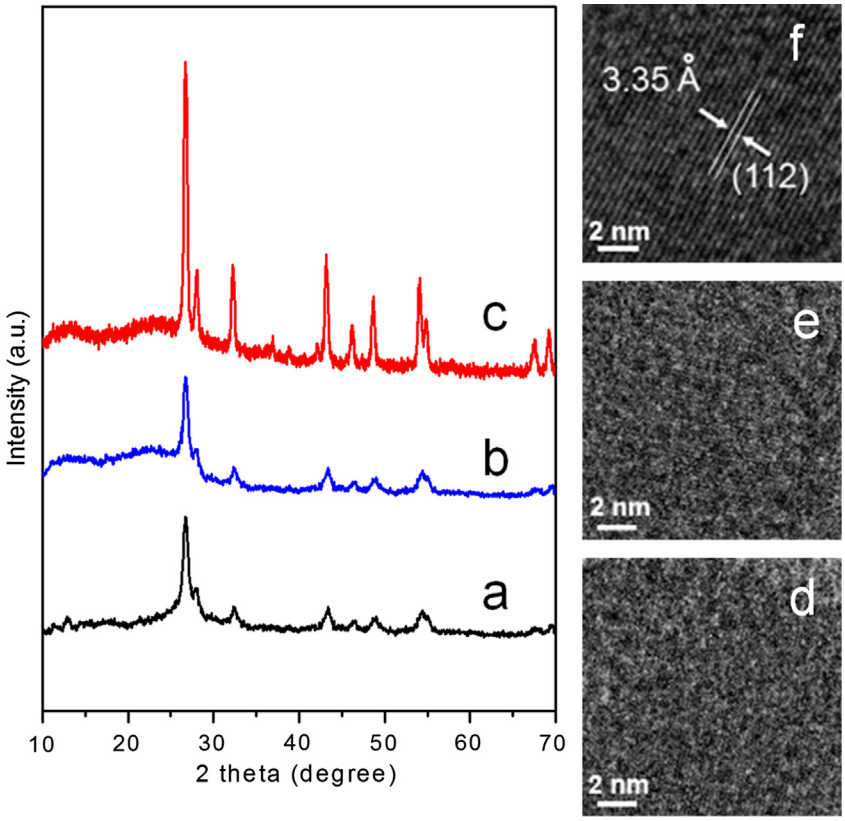

Fig. 3. XRD patterns of (a) bare $BaMoO_4$, (b) uncalcined $BaMoO_4@SiO_2$ and (c) calcined $BaMoO_4@SiO_2$. HRTEM images of the core of (d) bare $BaMoO_4$, (e) uncalcined $BaMoO_4@SiO_2$ and (f) calcined $BaMoO_4@SiO_2$.

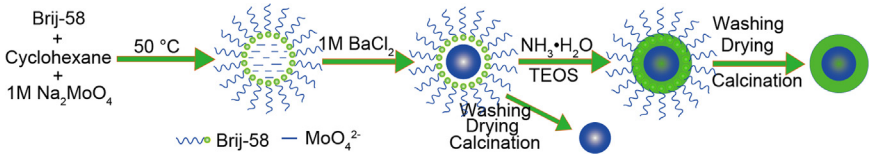

Scheme 1. Illustration of the formation process of core–shell $BaMoO_4@SiO_2$.

was formed through the hydrolysis and condensation of TEOS under the catalysis of ammonium hydroxide. After washing, drying, and calcination, water and organic compositions were removed. At the same time, the crystallinity of the $BaMoO_4$ cores was improved, as shown by the variation of XRD patterns and the appearance of lattice fringes in HRTEM images. Core–shell $BaMoO_4@SiO_2$ nanomaterials were thus formed.

3.3. Optical properties of nano core–shell $BaMoO_4@SiO_2$

To investigate the influence of coating and shell thickness on PL intensity, uncoated $BaMoO_4$ and $BaMoO_4@SiO_2$ with different shell thicknesses were dispersed in water and analyzed by UV–vis and PL spectroscopy (Fig. 4a). Their concentrations were carefully adjusted to ensure that the absorbance values at 209 nm (the maximum wavelength) were identical. From Fig. 4a, we can see that a silica coating could significantly enhance the PL intensity. The coated $BaMoO_4$ showed bright blue color under UV light, whereas the uncoated particles were hardly visible (Fig. 4c and d). The PL intensity of SiO_2-coated NPs with shells of 12 and 18 nm were enhanced by factors of 8.0 and 6.8, respectively. From this we can conclude that silica shell can increase the PL intensity, but the shell is not the thicker the better.

The reason for such a phenomenon can be deduced as follows. It is well known that the surface of bare $BaMoO_4$ synthesized at low temperatures contains many defects, which may cause non-radiative transition and decrease the PL intensity. Silica coating could reduce or eliminate the surface defects by reducing the number of dangling bonds on the nanoparticle surface. Thus, the surface was passivated and the PL intensity was enhanced [31]. However, light can be absorbed upon passing through silica [24]. According to the Lambert law, the transmission intensity of incident light will decrease with increasing absorption layer thickness. Therefore, for the thin shells the reduction of surface defects is the dominant factor, resulting in the enhancement of the PL

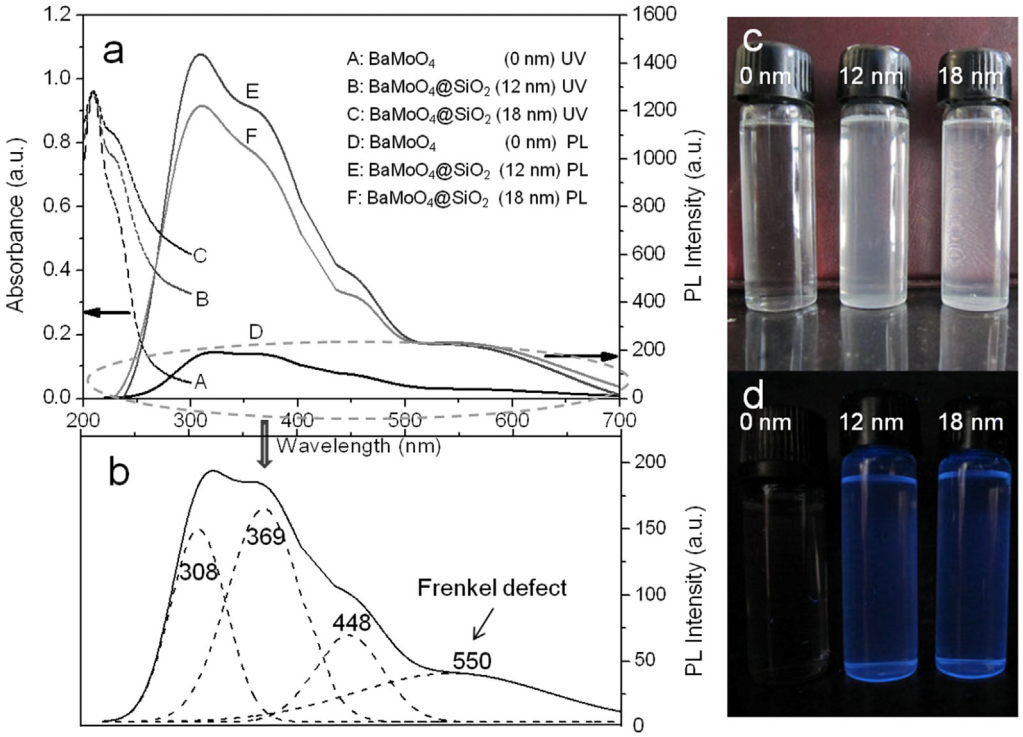

Fig. 4. (a) Absorption and emission spectra of uncoated $BaMoO_4$ and $BaMoO_4@SiO_2$ with different shell thicknesses. (b) Decomposed Gaussian components of bare $BaMoO_4$. Photographs of the uncoated $BaMoO_4$ and $BaMoO_4@SiO_2$ solutions under (c) ambient light and (d) UV light at 365 nm. (To see the blue PL color in Fig. 4d, the reader is referred to the web version of this article).

intensity. For the thick shells, the absorption effect becomes dominant. Hence, the PL intensity increases first and then decreases with the increase in the shell thickness.

As to the luminescence mechanism, it is generally known that the PL emission of the metal molybdates is mainly due to the charge-transfer transitions within the $[MoO_4^{2-}]$ complex [7]. Due to the Jahn–Teller splitting effect on the excited states of the tetrahedral $[MoO_4^{2-}]$ anion, the fluorescence emission spectrum is composed of several peaks overlapping each other and shows a broad peak. As we can see from Fig. 4a, all PL spectra show broad peaks, which can be decomposed into three individual Gaussian components: 308, 369, and 448 nm (Fig. 4b, the fourth Gaussian component at 550 nm is attributed to the Frenkel defect structure). Compared with reported data [7,9,15], where the main emission peaks are in visible region, apparent blue shift was observed due to quantum size effect, making the main emission peaks enter UV region. It is worth noting that while the emission at 448 nm makes the material emit blue light, the UV emissions at 308 and 369 nm might make the core–shell $BaMoO_4@SiO_2$ an active material for UV photonic devices.

4. Conclusions

In summary, nano core–shell $BaMoO_4@SiO_2$ with a core of 16–17 nm and shells of 12 and 18 nm were synthesized in a w/o microemulsion of Brij-58/cyclohexane/water. The shell thickness was tuned by varying the amounts of TEOS. We then investigated the PL intensity of $BaMoO_4$ with different shell thicknesses and found that the PL intensity of $BaMoO_4$ could be greatly enhanced by coating a silica layer with appropriate thickness. UV emissions at 308 and 369 nm were observed besides a visible blue emission at 448 nm, making the core–shell $BaMoO_4@SiO_2$ a promising candidate for UV photonic devices. Further we think that our synthetic strategy and PL enhancement effect can be facilely extended to other silica coated scheelite structured molybdates and tungstates, such as $CaMoO_4@SiO_2$, $PbWO_4@SiO_2$, etc., due to the structural and chemical similarity.

Acknowledgments

This work is supported by the National Natural Science Foundation of China (Grants nos. 20976023 and 21176038). The authors also would like to thank DUT Chemistry Analysis & Research Center for the contributions on the material characterization, and Zameer Hussain Shah for revising the language of the paper.

References

[1] F. Lei, B. Yan, H.-H. Chen, Q. Zhang, J.-T. Zhao, Surfactant-assisted hydrothermal synthesis, physical characterization, and photoluminescence of $PbWO_4$, Crystal Growth and Design 9 (2009) 3730–3736.

[2] Y. Hu, W. Zhuang, H. Ye, D. Wang, S. Zhang, X. Huang, A novel red phosphor for white light emitting diodes, Journal of Alloys and Compounds 390 (2005) 226–229.

[3] F. Lei, B. Yan, Hydrothermal synthesis and luminescence of $CaMO_4$:RE^{3+} (M=W, Mo; RE=Eu, Tb) submicro-phosphors, Journal of Solid State Chemistry 181 (2008) 855–862.
[4] G.-J. Xing, R. Liu, C. Zhao, Y.-L. Li, Y. Wang, G.-M. Wu, Photoluminescence and photocatalytic properties of uniform $PbMoO_4$ polyhedral crystals synthesized by microemulsion-based solvothermal method, Ceramics International 37 (2011) 2951–2956.
[5] V.B. Mikhailik, H. Kraus, G. Miller, M.S. Mykhaylyk, D. Wahl, Luminescence of $CaWO_4$, $CaMoO_4$, and $ZnWO_4$ scintillating crystals under different excitations, Journal of Applied Physics 97 (2005) 083523.
[6] M. Mai, C. Feldmann, Microemulsion-based synthesis and luminescence of nanoparticulate $CaWO_4$, $ZnWO_4$, $CaWO_4$:Tb, and $CaWO_4$:Eu, Journal of Materials Science, 47, 1427–1435.
[7] J.W. Yoon, J.H. Ryu, K.B. Shim, Photoluminescence in nanocrystalline $MMoO_4$ (M=Ca, Ba) synthesized by a polymerized complex method, Materials Science and Engineering B 127 (2006) 154–158.
[8] J.H. Ryu, K.M. Kim, S.W. Mhin, G.S. Park, J.W. Eun, K.B. Shim, C.S. Lim, Laser-induced synthesis of $BaMoO_4$ nanocolloidal suspension and its optical properties, Applied Physics A 92 (2008) 407–412.
[9] A. Phuruangrat, T. Thongtem, S. Thongtem, Barium molybdate and barium tungstate nanocrystals synthesized by a cyclic microwave irradiation, Journal of Physics and Chemistry of Solids 70 (2009) 955–959.
[10] J.C. Sczancoski, L.S. Cavalcante, N.L. Marana, R.O. da Silva, R.L. Tranquilin, M.R. Joya, P.S. Pizani, J.A. Varela, J.R. Sambrano, M. Siu Li, E. Longo, J. Andrés, Electronic structure and optical properties of $BaMoO_4$ powders, Current Applied Physics 10 (2010) 614–624.
[11] R.F. Service, Will UV lasers beat the blues? Science 276 (1997) 895.
[12] B. Liu, C.W. Cheng, R. Chen, Z.X. Shen, H.J. Fan, H.D. Sun, Fine structure of ultraviolet photoluminescence of tin oxide nanowires, Journal of Physical Chemistry C 114 (2010) 3407–3410.
[13] J.H. Jun, H. Seong, K. Cho, B.-M. Moon, S. Kim, Ultraviolet photodetectors based on ZnO nanoparticles, Ceramics International 35 (2009) 2797–2801.
[14] L. Tang, R. Ji, X. Cao, J. Lin, H. Jiang, X. Li, K.S. Teng, C.M. Luk, S. Zeng, J. Hao, S.P. Lau, Deep ultraviolet photoluminescence of water-soluble self-passivated graphene quantum dots, ACS Nano 6 (2012) 5102–5110.
[15] L.S. Cavalcante, J.C. Sczancoski, R.L. Tranquilin, M.R. Joya, P.S. Pizani, J.A. Varela, E. Longo, $BaMoO_4$ powders processed in domestic microwave-hydrothermal: synthesis, characterization and photoluminescence at room temperature, Journal of Physics and Chemistry of Solids 69 (2008) 2674–2680.
[16] C.F. Hoener, K.A. Allan, A.J. Bard, A. Campion, M.A. Fox, T.E. Mallouk, S.E. Webber, J.M. White, Demonstration of a shell–core structure in layered cadmium selenide–zinc selenide small particles by x-ray photoelectron and Auger spectroscopies, Journal of Physical Chemistry 96 (1992) 3812–3817.
[17] R. Ghosh Chaudhuri, S. Paria, Core/shell nanoparticles: classes, properties, synthesis mechanisms, characterization, and applications, Chemical Reviews 112 (2011) 2373–2433.
[18] L.M. Liz-Marzan, M. Giersig, P. Mulvaney, Homogeneous silica coating of vitreophobic colloids, Chemical Communications (1996) 731–732.
[19] T. Nann, P. Mulvaney, Single quantum dots in spherical silica particles, Angewandte Chemie International Edition 43 (2004) 5393–5396.
[20] A. Cao, R. Lu, G. Veser, Stabilizing metal nanoparticles for heterogeneous catalysis, Physical Chemistry Chemical Physics 12 (2010) 13499–13510.
[21] A. Guerrero-Martínez, J. Pérez-Juste, L.M. Liz-Marzán, Recent progress on silica coating of nanoparticles and related nanomaterials, Advanced Materials 22 (2010) 1182–1195.
[22] H.M. Kuang, Z.X. Deng, C.H. Li, X.M. Sun, J. Zhuang, Y.D. Li, Synthesis and photoluminescent properties of CdS/SiO_2 nanorod core–shell structure, Acta Physico-Chimica Sinica 18 (2002) 477–480.
[23] X. Zhou, Y. Kobayashi, V. Romanyuk, N. Ochuchi, M. Takeda, S. Tsunekawa, A. Kasuya, Preparation of silica encapsulated CdSe quantum dots in aqueous solution with the improved optical properties, Applied Surface Science 242 (2005) 281–286.
[24] Q. Lu, F. Guo, L. Sun, A. Li, Surface modification of ZrO_2:Er^{3+} nanoparticles to attenuate aggregation and enhance upconversion fluorescence, Journal of Physical Chemistry C 112 (2008) 2836–2844.
[25] Q. Lu, F. Guo, L. Sun, A. Li, L. Zhao, Silica-/titania-coated Y_2O_3:Tm^{3+}, Yb^{3+} nanoparticles with improvement in upconversion luminescence induced by different thickness shells, Journal of Applied Physics 103 (2008) 123533.
[26] S. Liu, M.Y. Han, Silica-coated metal nanoparticles, Chemistry—An Asian Journal 5 (2010) 36–45.
[27] Y. Han, J. Jiang, S.S. Lee, J.Y. Ying, Reverse microemulsion-mediated synthesis of silica-coated gold and silver nanoparticles, Langmuir 24 (2008) 5842–5848.
[28] Y. Yang, L. Jing, X. Yu, D. Yan, M. Gao, Coating aqueous quantum dots with silica via reverse microemulsion method: toward size-controllable and robust fluorescent nanoparticles, Chemistry of Materials 19 (2007) 4123–4128.
[29] J. Wang, X. Li, S. Zhang, R. Lu, Facile synthesis of ultrasmall monodisperse raisin bun-type MoO_3/SiO_2 nanocomposites with enhanced catalytic properties, Nanoscale 5 (2013) 4823–4828.
[30] L. Yang, R. Xie, L. Liu, D. Xiao, J. Zhu, Synthesis and characterization of ZnSe nanocrystals by W/O reverse microemulsion method: the effect of cosurfactant, Journal of Physical Chemistry C 115 (2011) 19507–19512.
[31] M. Nirmal, L. Brus, Luminescence photophysics in semiconductor nanocrystals, Accounts of Chemical Research 32 (1998) 407–414.